

Two-component wind fields from single scanning aerosol lidar

Shane D. Mayor^a, Pierre Dérian^a, Christopher F. Mauzey^a, and Masaki Hamada^a

^aCalifornia State University Chico, Chico, California, USA

ABSTRACT

An overview of recent research results on the performance of two motion estimation algorithms used to deduce two-component horizontal wind fields from ground-based scanning elastic backscatter lidar is presented. One motion estimation algorithm is a traditional cross-correlation method optimized for atmospheric lidar data. The second algorithm is a recently-developed wavelet-based optical flow. An intercomparison of experimental results with measurements from an independent Doppler lidar over an agricultural area in Chico, California, during daytime convective conditions in 2013-14 are presented. Finally, early results from application of the algorithms to data collected over the ocean from a compact and portable aerosol lidar that was deployed on the northern California coast in March of 2015 are presented.

Keywords: lidar, aerosol, algorithms, motion estimation, cross-correlation, optical flow, turbulence, wind, surf

1. MOTIVATION

Vertical fluxes of heat, moisture, momentum, pollutants, and trace gases at the bottom of the atmosphere are dependent on the effectiveness of turbulence that is responsible for the transport. Fine-scale numerical simulations of the atmosphere are capable of resolving intricate details of the spatial structure of turbulence, the temporal evolution of the turbulence structure, and determining fluxes. However, observing technologies remain far behind the numerical simulations in terms of resolution, precision and area coverage. The motivation of our work is to develop instruments and algorithms that can provide the spatial observations required to validate fine-scale simulations. Trusted fine-scale simulations can then be used to develop parameterizations for models with coarser resolutions, such as those used in weather and climate prediction.

Techniques to observe the spatial distribution of all variables should be developed. In the present work, we focus on the two horizontal components of the wind field. The approach that we employ is very similar to particle image velocimetry (PIV) that is enormously successful in experimental fluid dynamics,¹ or to atmospheric motion vectors (AMVs) which are a key component of operational numerical weather prediction.² The differences between our atmospheric application and that of PIV is that the latter are almost always conducted in highly controlled laboratory environments, such as wind tunnels or tanks with deliberate seeding of the flow, and with cameras that provide a Cartesian array of pixels with approximately uniform signal to noise ratio (SNR). Here, we cannot control the flow or the tracers in the atmosphere. Lidar is the leading method for illuminating the naturally occurring tracers over substantial areas, but contrary to cameras scanning lidar data are obtained in a spherical coordinate system and have spatially and temporally variable SNR.

2. CROSS-CORRELATION

The cross-correlation algorithm (CCA) is a mainstay in the field of motion estimation. It is used to compute the apparent motion of objects and fluid flows in the fields of robotics, navigation, medical imaging, and geosciences.³⁻⁹ In the atmospheric sciences, the CCA has been applied to satellite imagery,^{10,11} radar data,¹² and lidar data.¹³⁻¹⁷ In our very recent work, we have investigated the integrity of the approach for turbulent near-surface atmospheric flows under ideal aerosol conditions using both synthetic fields and real data. In summary, we can state that because the CCA employs an “interrogation window”, it is likely not the best algorithm suited for resolving the finest scale turbulence structures. Use of the CCA assumes a uniformity of the flow within the interrogation window. Details of our research on the CCA can be found in the master’s thesis of Hamada¹⁸ and in a manuscript¹⁹ that is accepted pending revisions to the *Journal of Atmospheric and Oceanic Technology*. A flowchart describing the basic approach of the CCA is shown in Fig. 1.

Further author information:

S.D.M.: E-mail: sdmayor@csuchico.edu, Telephone: 1 530 898 6337

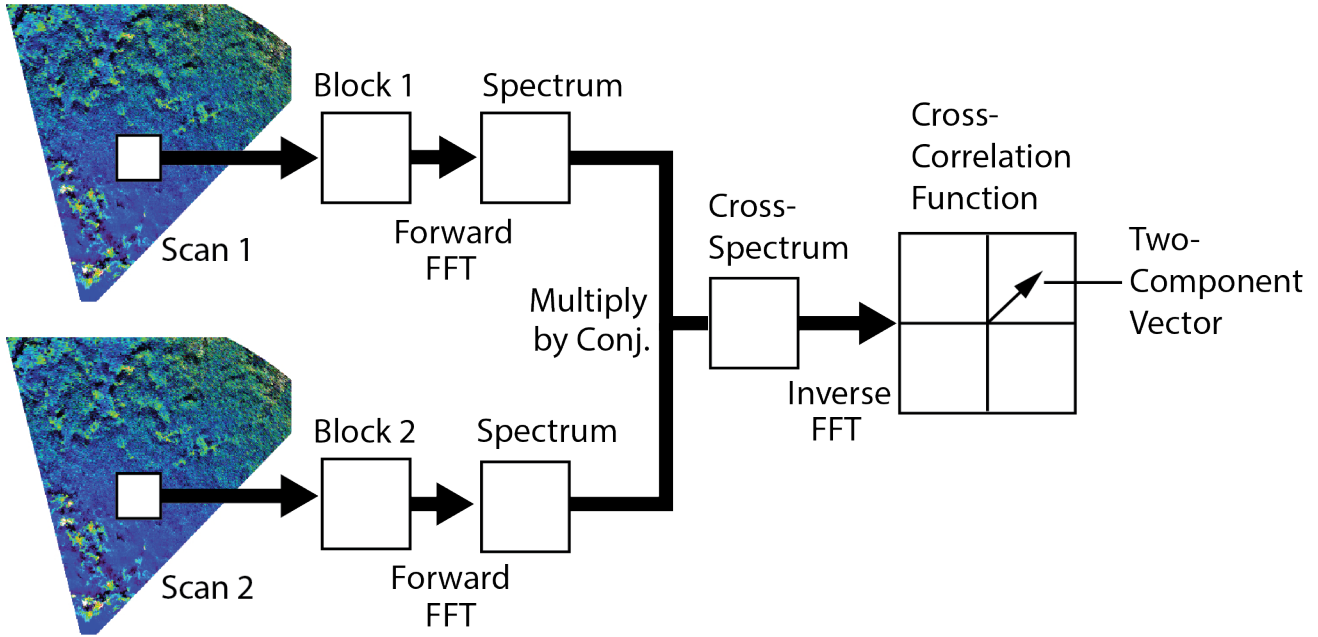


Figure 1: Flow chart description of the cross-correlation approach to motion estimation (for one vector). Block 1 and Block 2 are the subsets of pixels from the interrogation window.

3. WAVELET-BASED OPTICAL FLOW

Horn and Schunck²⁰ described in 1981 another approach to determining the motion field that, contrary to the cross-correlation method, does not involve an interrogation window but instead uses all pixels of both images to determine all vectors in the flow field simultaneously. The family of methods that were subsequently developed from this seminal work is called variational optical flow, often simply “optical flow” for short. Variational optical flow methods provide a dense and continuous representation of the motion, and have been applied to a wide range of situations, including fluid motion estimation.^{21–23} In 2012, Dérian^{24,25} published a novel variant of this variational approach that represents the motion on a multiscale wavelet basis. This algorithm was validated against actual and synthetic PIV data and outperformed the cross-correlations. Details of the adaptation of the wavelet-based optical flow to accommodate the unique characteristics of lidar data and experimental results are described by Dérian et al.²⁶ A flowchart describing the basic approach is shown in Fig. 2.

4. VALIDATION EXPERIMENT

The CCA and wavelet-based optical flow algorithm were implemented to take advantage of the massively parallel architecture of general purpose graphical processing units (GPUs).²⁷ The CCA was named *Gale* and the wavelet-based optical flow was named *Typhoon*. Using the GPUs, the execution time is small enough to compute flow fields within the time it takes the lidar to make one scan, typically about 10–20 s.

To test the ability of the algorithms to determine the vector wind fields, an experiment was conducted in Chico, California, in 2013–14. A commercially-available, compact Doppler lidar was used to provide independent validation. The lidar used to image the aerosol fields was the original NSF Raman-shifted Eye-safe Aerosol Lidar (REAL).^{28–30} The Doppler lidar was located 1523 m range and a heading of 15° from the REAL. It operated in a mast-replacement mode providing horizontal wind vectors between 30 and 170 m at 10 m intervals from a repeating sequence of 4 inclined beams and one vertical beam every 17 s. The REAL collected a nearly-horizontal sector scan between -15° and 45° azimuth every 17 s. The elevation angle of the PPI sector scans was typically 4° above the horizon in order to place the scan at 100 m AGL at the location of the Doppler lidar (see Fig. 3).

Figure 4 shows the vector flow fields resulting from *Gale* (left) and *Typhoon* (right). Both flow fields are superimposed on the high-pass median filtered elastic backscatter data in shades of copper. This data was

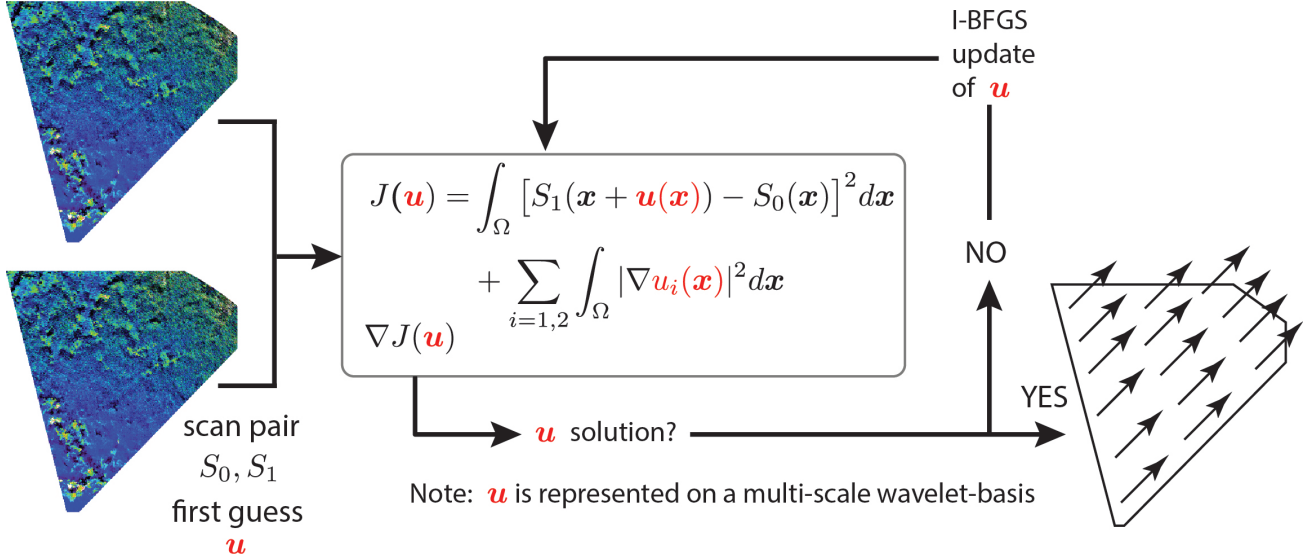


Figure 2: Flow chart description of the wavelet-based optical flow approach to motion estimation. I-BFGS stands for iterative Broyden-Fletcher-Goldfarb-Shanno (BFGS) algorithm and it is a method for solving unconstrained nonlinear optimization problems.

collected at 23:32 UTC on 23 October 2013 at the California State University Chico Farm. Winds were light and variable during this time and the atmosphere was convective. The flow fields shown in Fig. 4 were computed from just two PPI sector scans of the REAL separated by 17 s. Of particular interest in the flow field is a microscale vortex that passed over the region moving from the SW to the NE. Vortices such as these are routinely observed in the flow fields from large eddy simulations.³¹

The experimental arrangement enabled us to perform extensive time-series comparisons like those shown in Figs. 5 and 6. In general, we found that the motion estimation approach to measuring winds (over land at 100 m AGL) tends to fail at night when the atmosphere becomes stability stratified resulting in the absence of aerosol plumes to serve as tracers of the flow. However, during the daylight hours, when the static stability decreases and turbulence mixing occurs, plume structure emerges and the approach works well. Statistics such as root mean squared differences and correlation coefficients between the motion estimates and the Doppler lidar measurements during ideal daytime aerosol conditions were computed for 10-min averages and are presented in Hamada et al.¹⁹ and Dérian et al.²⁶ RMS errors on u (east-west) and v (north-south) components are on the order of 0.29 m s^{-1} for optical flow and 0.35 m s^{-1} for cross-correlation. Correlation coefficients are greater than 0.99 for both methods. The slope of the linear fit for the u and v components for cross-correlation is 0.974 and 0.991, respectively. The slope of the linear fit for the u and v components for optical flow is 0.989 and 1.001, respectively. Estimates of velocity transfer functions showing the spatial resolution of the velocity components from Typhoon are contained in Dérian et al.²⁶ The transfer functions indicate that the approach begins to miss variance at scales in the range of 200 to 300 m and gradually decreases like a cosine taper towards smaller spatial scales.

5. OFFSHORE WINDS

A particularly important and challenging environment to observe and simulate is that of the turbulent atmosphere over rough ocean surfaces.^{32,33} Atmospheric simulations over oceans are challenging because, unlike terrain, the fluid bottom boundary moves vertically, and it does so quickly. Observations are challenging because of the difficulty of placing sensors near large amplitude and breaking waves in the open ocean especially during high wind conditions. A compact elastic backscatter lidar named SAMPLE was validated against the REAL in Chico, California, from 9-20 March 2015.³⁴ The SAMPLE was then transported to the northern California coast and deployed on various beaches there from 21-31 March 2015. The goal of the 10-day pilot experiment

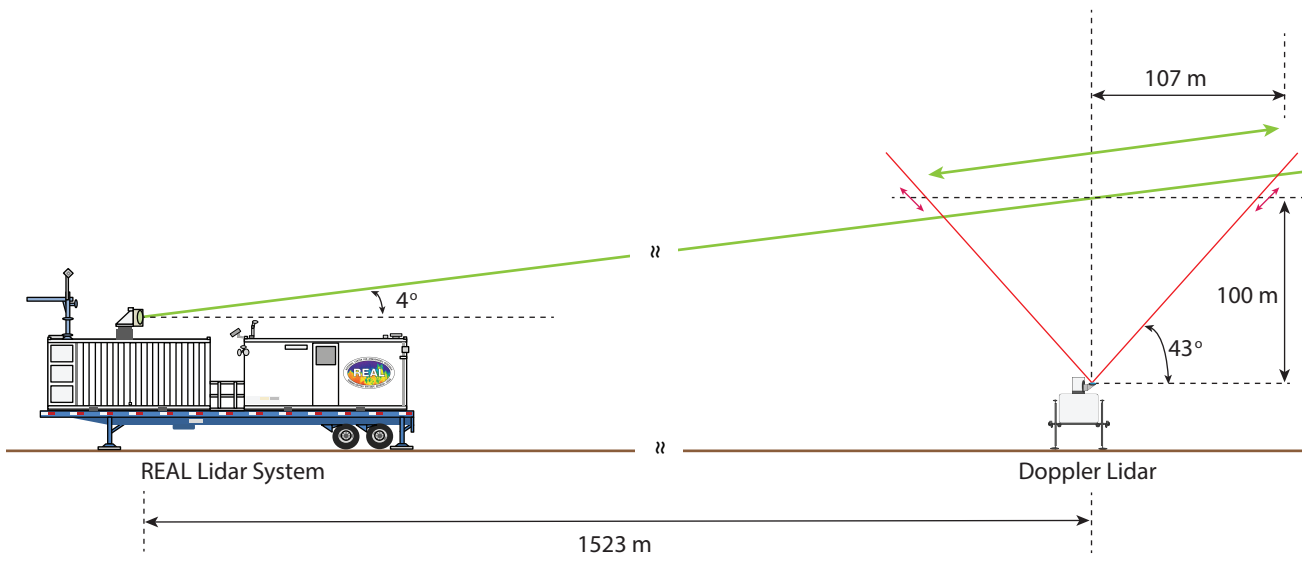


Figure 3: Diagram showing the vertical geometry of the 2013-14 field experiment in Chico, California. Distances shown are not to scale.

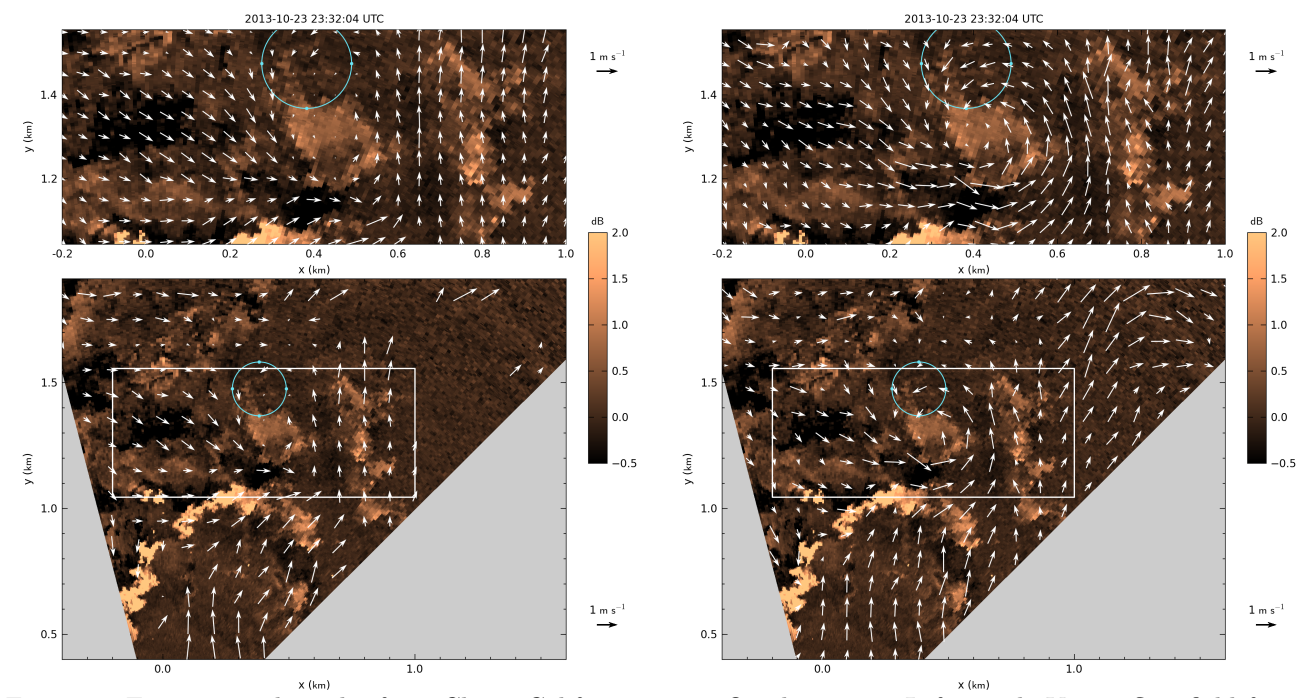


Figure 4: Experimental results from Chico, California on 23 October 2013. Left panel: Vector flow field from the cross-correlation algorithm. Right panel: Vector flow field from the wavelet-based optical flow algorithm. The top panels are expansions of the area outlined by the white rectangle in the lower panels. The light blue dots on the light blue circle represent the sample volumes of the Doppler lidar at 100 m AGL. Vectors shown are subsampled from the full vector fields for clarity. A microscale vortex can be observed near the middle of the scan area.

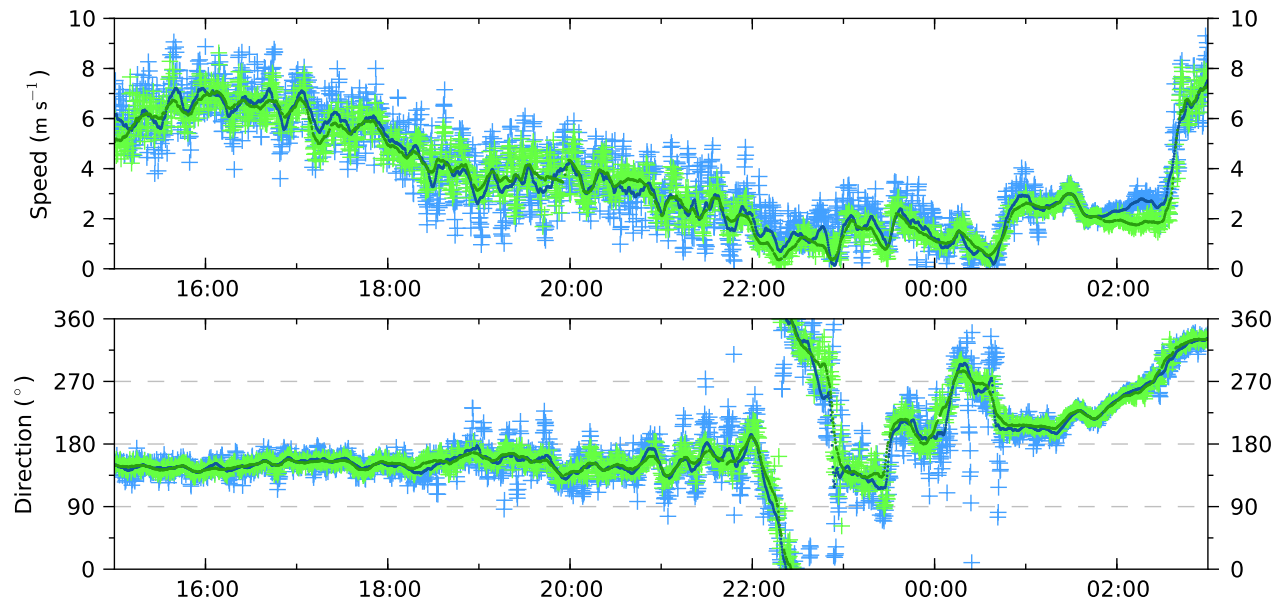


Figure 5: Time-series from Gale (green) and the Doppler lidar (blue). Individual measurements are shown with + symbols. Solid lines represent 10-minute running means.

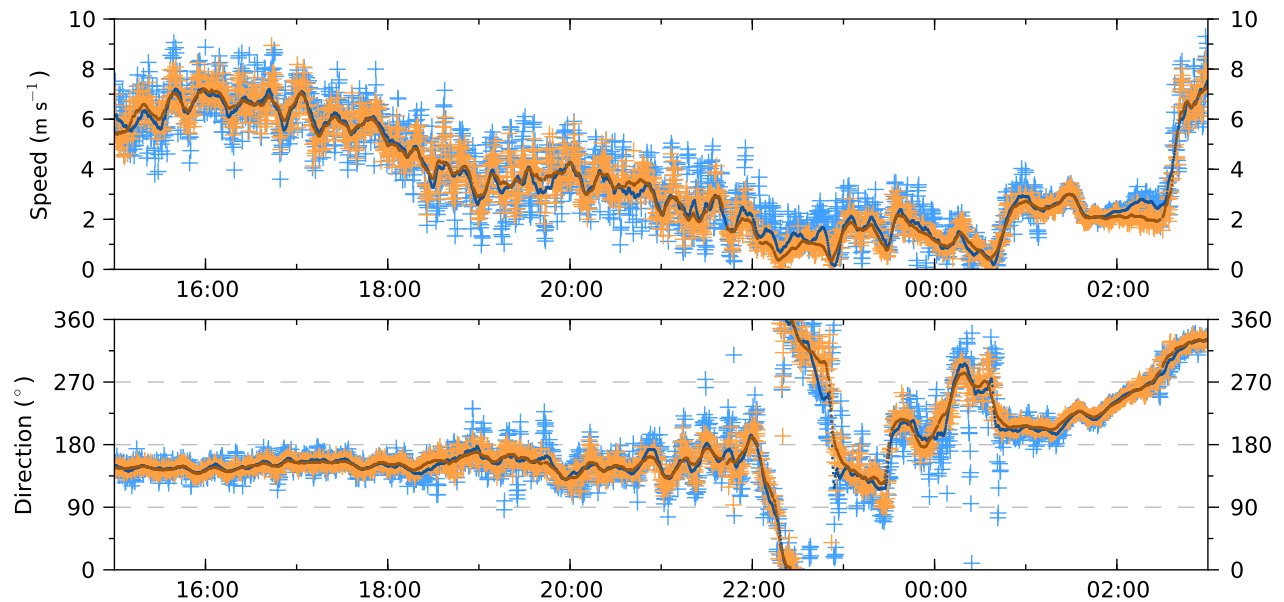


Figure 6: Time-series from Typhoon (orange) and the Doppler lidar (blue). Individual measurements are shown with + symbols. Solid lines represent 10-minute running means.

was to determine whether a compact micropulse lidar like the SAMPLE could be used to observe spray from breaking waves and estimate the wind field over rough ocean surfaces. The Pacific Ocean along the northern California coast is notoriously rough but unfortunately the weather conditions were such that we only observed high amplitude sea states (2.4 – 3.6 m) on the last day of the experiment.

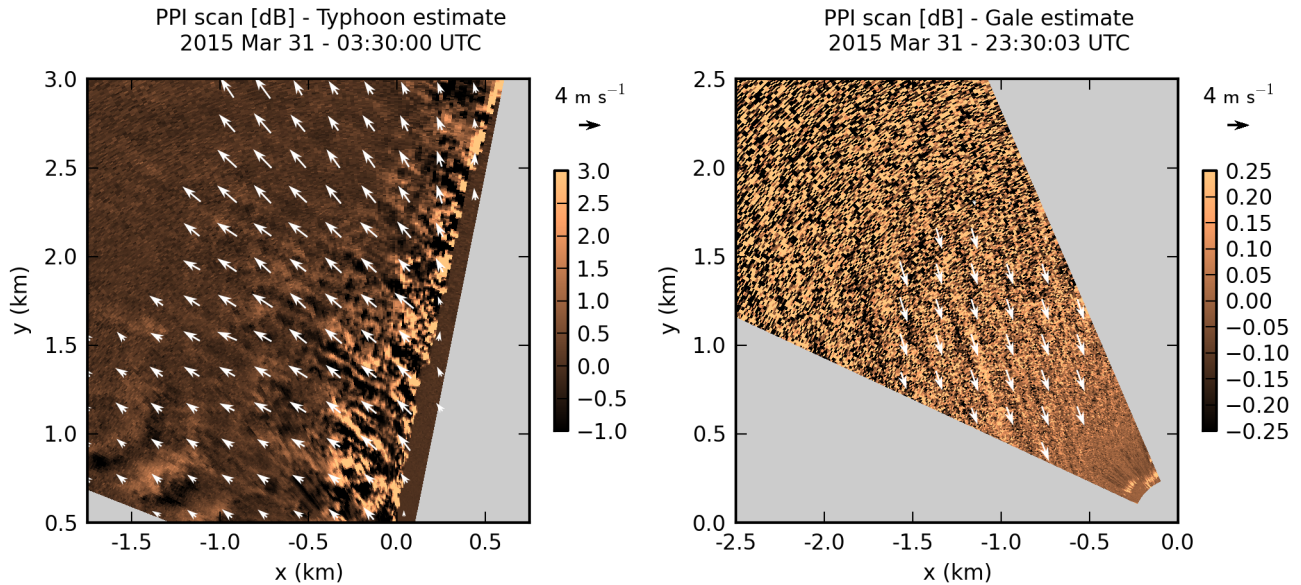


Figure 7: Left panel: SAMPLE observations of offshore wind and aerosol from Big Lagoon County Park, California. Plumes of particulate matter generated by breaking waves along the beach enable the observation of the offshore flow field at this time. Right panel: SAMPLE observations of wind and aerosol from Samoa, California, during a period with 2.4 – 3.6 m amplitude waves. Despite the large waves, whitecaps were sparse and fleeting beyond the surf zone. Particulate matter was organized into long streaky structures.

The SAMPLE was so compact that it was deployed from the back of a U-Haul moving van and powered by a small gasoline generator. The van was parked at public parking lots within meters of the beach and the ocean. The SAMPLE scanned mostly horizontally to observe the aerosol and wind field just above the ocean and occasionally vertically to reveal marine boundary layer structure. The horizontal scans were just meters above the crests of the waves. Fig. 7 shows SAMPLE observations over the ocean from two periods less than a day apart with different atmospheric and oceanic conditions. The left panel is a sector scan that was collected in the early evening at Big Lagoon County Park (11.5 km north of Trinidad, California) when no whitecaps were observed beyond the surf zone. The bright plume structure along the right side of the sector scan is the result of ocean waves breaking along the beach. The motion estimation algorithms were able to derive the offshore wind field advecting these coherent plume structures to more than 1 km offshore. The left panel of Fig. 7 proves that the SAMPLE can detect sufficient aerosol structure from breaking waves and suggests that the plume structure can be used to determine the flow field.

The right panel of Fig. 7 was collected during the afternoon of the subsequent day from a deployment location in Samoa, California, that is 41 km south of Big Lagoon County Park. A synoptic scale cold front had passed over the region between the two observation periods resulting in a dramatic shift in the wind. The wind in the right panel is from the northwest and the amplitude of the ocean was much larger than the previous evening. The elastic backscatter field shows narrow and elongated aerosol plume structures that resemble streaks³⁵ typically observed in model output of neutral-stability shear-driven flows. Visibility during the 31st was high and white caps beyond the surf zone were very sparse and fleeting. Therefore, this period was challenging for any lidar. We expect that if more whitecaps had been present, the aerosol structure would have been more pronounced and the wind field retrievals better.

6. SUMMARY

Five general points are worth pointing out. First, a new wavelet-based optical flow motion estimation algorithm (named Typhoon) has been developed and it appears to be able to resolve smaller scale velocity features than cross-correlation. Second, by comparing the velocity estimates with those from a Doppler lidar, an accepted standard for wind measurement, we have begun to quantify accuracy and precision. In addition (third), we have estimated the spatial resolution of the Typhoon velocity fields by computing spatial power spectra and comparing those spectra with estimates based on Kolmogorov's inertial subrange hypothesis. However, many factors influence the accuracy, precision and resolution of the retrieved vector fields and much more work remains to be done on this topic. For example, the mechanism by which turbulence is generated (shear or buoyancy) have a profound effect on the turbulence structure which in turn effects plume structure and retrieval of the flow fields. Furthermore, it may be possible to increase the spatial resolution of the flow fields by adjusting the scan rate and azimuthal range of the lidar scans. Fourth, a new and compact elastic backscatter lidar has become available that can be used economically to probe the aerosol field just above wave crests. Further improvements in lidar performance are likely. Finally, a pilot experiment confirmed the hypothesis that the particulate matter generated by breaking ocean waves is more than adequate for such a lidar to detect. In the future, we wish to deploy a SAMPLE with a suite of other instruments on the coast and observe rough oceans with abundant whitecaps. We will use these observations to validate simulations of lower atmosphere turbulence structure and advance theories on air-sea interaction.

ACKNOWLEDGMENTS

This work was supported by the National Science Foundation's Physical and Dynamic Meteorology Program under awards AGS 0924407 and 1228464. Deployment of the SAMPLE in Chico CA in March 2015 was supported by HDTRA2-15-C-0003. Deployment of the SAMPLE in Eureka CA in March 2015 was supported by NSF AGS 1536624.

REFERENCES

- [1] Gurka, R. and Kit, E., "Optical methods and unconventional experimental setups in turbulence research," in [*Handbook of Environmental Fluid Dynamics, Vol. 2*], Fernando, H. J. S., ed., CRC Press/Taylor and Francis Group, LLC. (2013).
- [2] Velden, C., Daniels, J., Stettner, D., Santek, D., Key, J., Dunion, J., Holmlund, K., Dengel, G., Bresky, W., and Menzel, P., "Recent innovations in deriving tropospheric winds from meteorological satellites," *Bulletin of the American Meteorological Society* **86**(2), 205–223 (2005).
- [3] Murray, J. C., Erwin, H. R., and Wermter, S., "Robotic sound-source localisation architecture using cross-correlation and recurrent neural networks," *Neural Networks* **22**(2), 173–189 (2009).
- [4] Emery, W. J., Baldwin, D., and Matthews, D., "Maximum cross correlation automatic satellite image navigation and attitude corrections for open-ocean image navigation," *IEEE T. Geosci. Remote Sens.* **41**(1), 33–42 (2003).
- [5] Avants, B. B., Epstein, C. L., Grossman, M., and Gee, J. C., "Symmetric diffeomorphic image registration with cross-correlation: evaluating automated labeling of elderly and neurodegenerative brain," *Med. Image Anal.* **12**(1), 26–41 (2008).
- [6] Schubert, A., Faes, A., Kääb, A., and Meier, E., "Glacier surface velocity estimation using repeat TerraSAR-X images: Wavelet vs. correlation-based image matching," *Int. Soc. Photogramme.* **82**, 49–62 (2013).
- [7] Adrian, R. J. and Westerweel, J., [*Particle Image Velocimetry*], Cambridge University Press (2011).
- [8] Cheng, W., Murai, Y., Sasaki, T., and Yamamoto, F., "Bubble velocity measurement with a recursive cross correlation PIV technique," *Flow Meas. Instrum.* **16**(1), 35–46 (2005).
- [9] Antoine, E., Buchanan, C., Fezzaa, K., Lee, W.-K., Rylander, M. N., and Vlachos, P., "Flow measurements in a blood-perfused collagen vessel using x-ray micro-particle image velocimetry," *PLOS ONE* **8**(11), e81198 (2013).
- [10] Leese, J. A., Novak, C. S., and Clark, B. B., "An automated technique for obtaining cloud motion from geosynchronous satellite data using cross correlation," *J. Appl. Meteorol.* **10**(1), 118–132 (1971).

- [11] García-Pereda, J. and Borde, R., “The impact of the tracer size and the temporal gap between images in the extraction of atmospheric motion vectors,” *J. Atmos. Ocean. Technol.* **31**(8), 1761 – 1770 (2014).
- [12] Rinehart, R. E. and Garvey, E. T., “Three-dimensional storm motion detection by conventional weather radar,” *Nature* **273**, 287–289 (1978).
- [13] Eloranta, E. W., King, J. M., and Weinman, J. A., “The determination of wind speeds in the boundary layer by monostatic lidar,” *J. Appl. Meteor.* **14**, 1485–1489 (1975).
- [14] Shimizu, H., Sasano, Y., Yasuoka, Y., Ueda, H., Takeuchi, N., and Okuda, M., “The remote measurement of wind direction and velocity by a laser radar using the spatial correlation technique,” *Oyobutsuri* **50**, 616–620 (1981).
- [15] Kolev, I., Parvanov, O., and Kaprielov, B., “Lidar determination of winds by aerosol inhomogeneities: motion velocity in the planetary boundary layer,” *Appl. Optics* **27**, 2524–2531 (1988).
- [16] Mayor, S. D. and Eloranta, E. W., “Two-dimensional vector wind fields from volume imaging lidar data,” *J. Appl. Meteor.* **40**, 1331–1346 (2001).
- [17] Mayor, S. D., Lowe, J. P., and Mauzey, C. F., “Two-component horizontal aerosol motion vectors in the atmospheric surface layer from a cross-correlation algorithm applied to scanning elastic backscatter lidar data,” *J. Atmos. Ocean. Technol.* **29**, 1585–1602 (2012).
- [18] Hamada, M., *Evaluation of the performance of a cross-correlation algorithm for wind velocity estimation using synthetic backscatter lidar images and velocity fields*, diploma thesis, California State University, Chico, 400 West First Street, Chico CA 95929 (Aug 2014).
- [19] Hamada, M., Dérian, P., Mauzey, C. F., and Mayor, S. D., “Optimization of the cross-correlation algorithm for two-component wind field estimation from single aerosol lidar data and comparison with Doppler lidar,” *Submitted to J. Atmos. Ocean. Technol.* (2015).
- [20] Horn, B. K. P. and Schunck, B. G., “Determining optical flow,” *Artificial Intelligence* **17**, 185–203 (1981).
- [21] Heitz, D., Mémin, E., and Schnörr, C., “Variational fluid flow measurements from image sequences: synopsis and perspectives,” *Experiments in Fluids* **48**(3), 369–393 (2010).
- [22] Corpetti, T., Heitz, D., Arroyo, G., Mémin, E., and Santa-Cruz, A., “Fluid experimental flow estimation based on an optical-flow scheme,” *Exp. Fluids* **40**(1), 80–97 (2006).
- [23] Dérian, P., Héas, P., Mémin, E., and Mayor, S. D., “Dense motion estimation from eye-safe aerosol lidar data,” in *Proceedings of the 25th International Laser Radar Conference*, **1**, 377–380 (2010).
- [24] Dérian, P., *Wavelets and Fluid Motion Estimation*, PhD thesis, MATISSE, Université Rennes 1 (2012). [Available online at http://tel.archives-ouvertes.fr/tel-00761919/PDF/theseDERIAN_v3.BU_.pdf].
- [25] Dérian, P., Héas, P., Herzet, C., and Mémin, E., “Wavelets and optical flow motion estimation,” *Numerical Mathematics Theory, Methods, and Applications* (2012).
- [26] Dérian, P., Mauzey, C. F., and Mayor, S. D., “Wavelet-based optical flow for two-component wind field estimation from single aerosol lidar data,” *J. Atmos. Ocean. Technol. (In Press)* (2015).
- [27] Mauzey, C. F., Lowe, J. P., and Mayor, S. D., “Real-time wind velocity estimation from aerosol lidar data using graphics hardware,” GPU Technology Conference, San Jose, CA (May 2012). Poster presentation AV10.
- [28] Mayor, S. D. and Spuler, S. M., “Raman-shifted Eye-safe Aerosol Lidar,” *Appl. Optics* **43**, 3915–3924 (2004).
- [29] Spuler, S. M. and Mayor, S. D., “Scanning eye-safe elastic backscatter lidar at 1.54 microns,” *J. Atmos. Ocean. Technol.* **22**, 696–703 (2005).
- [30] Mayor, S. D., Spuler, S. M., Morley, B. M., and Loew, E., “Polarization lidar at 1.54-microns and observations of plumes from aerosol generators,” *Opt. Eng.* **46**, DOI: 10.1117/12.781902 (2007).
- [31] Kanak, K. M., “Numerical simulation of dust devil-scale vortices,” *Quart. J. R. Met. Soc.* **131**(607), 1271–1292 (2005).
- [32] Mayor, S. D., Dérian, P., Mauzey, C. F., and Hamada, M., “Observations of two-component wind fields from aerosol lidar and motion estimation algorithms including first results over rough sea states,” International Conference on Model Integration across Disparate Scales in Complex Turbulent Flow Simulation (June 2015). Paper 28.
- [33] Sullivan, P. P., McWilliams, J. C., and Patton, E. G., “Large-eddy simulation of martine atmospheric boundary layers above a spectrum of moving waves,” *J. Atmos. Sci.* **71**, 4001–4027 (2014).

- [34] Mayor, S. D., Dérian, P., Mauzey, C. F., Spuler, S. M., Ponsardin, P., Pruitt, J., Ramsey, D., and Higdon, N. S., “Comparison of aerosol backscatter and wind field estimates from REAL and SAMPLE,” SPIE (August 2015). Paper 9612-16.
- [35] Drobinski, P. and Foster, R., “On the origin of near-surface streaks in the neutrally-stratified planetary boundary layer,” *Bound. Layer Meteor.* **108**(2), 247–256 (2003).